A Passive EKF-Based RIS-Aided Cellular Navigation System

Ali A. Abdallah

Electrical Engineering and Computer Science
University of California, Irvine
Irvine, California, USA
abdalla2@uci.edu

A. Lee Swindlehurst

Electrical Engineering and Computer Science
University of California, Irvine
Irvine, California, USA
swindle@uci.edu

Abstract—This paper presents a novel reconfigurable intelligent surface (RIS)-based localization approach for mobile user equipment (UE) in a millimeter-wave uplink cellular environment. The proposed approach develops a measurement engine that employs a state-of-the-art carrier-aided code-phasebased navigation receiver and incorporates a passive correlationbased angle-locked loop (ALL) for TOA and AOA estimation. An extended Kalman filter (EKF)-based RIS-aided navigation framework is deployed, providing accurate 3D position and velocity estimates for the mobile UEs utilizing the RIS-based navigation observables, which are then leveraged to optimize the RIS phase profile to maximize the signal-to-noise ratio (SNR) for the various UEs. Finally, the paper demonstrates the accuracy of the navigation solution through extensive Monte Carlo simulations that encompass different scenarios involving pedestrians, ground vehicles, and unmanned aerial vehicles (UAVs). These simulations emphasize the utility of our proposed approach in delivering sub-meter and meter-level positioning accuracies.

Index Terms—Intelligent Surfaces, Localization, Navigation

I. Introduction

The demand for accurate absolute positioning has driven the exploration of ambient radio signals for navigation. Cellular signals are considered a viable alternative/complementary source to GNSS for navigation [1]-[4], serving both navigation and wireless communication needs, especially in 5G systems [5]. Understanding the radio environment is crucial for signal-based navigation, as it involves extracting information from the sensed signals. Signal attenuation poses a significant challenge in radio environments, particularly for 5G and beyond, as their high-frequency signals have limited range and struggle to penetrate obstacles. While this limitation reduces multipath interference, which is desirable for navigation, it remains a challenge for communication purposes, where multipath can enhance the reliability of nonline-of-sight links. To address these propagation challenges, reconfigurable intelligent surfaces (RISs) have emerged as a promising technology. RISs are passive devices with electronically tunable reflection coefficients that enable favorable control of the RF propagation environment [6]-[8].

Extensive research has been conducted on the benefits of RISs for positioning and navigation. Various localization

This work was performed with financial assistance from U.S. National Science Foundation grants CCF-2225575 and ECCS-2030029.

schemes have been proposed using time-of-arrival (TOA), angle-of-arrival (AOA), angle-of-departure (AOD), or a combination of these measurements in conjunction with RISs to achieve accurate positioning [9]-[11]. Studies have shown that RISs can replace active access points (APs) in indoor positioning, with TOA measurements being more advantageous for position estimation [12]. In multi-user passive localization scenarios, dividing the RIS phase profile and selectively utilizing time-varying components based on orthogonal sequences can avoid interference and achieve sub-meter positioning accuracy [9]. Another approach investigates utilizing wavefront curvature in geometric near-field (NF) conditions, demonstrating the potential of inferring the UE's position solely from the RISreflected multipath component in the absence of a direct path [13]. For far-field (FF) scenarios, both line-of-sight (LOS) and non-line-of-sight (NLOS) paths are required for localization. Partially-connected receiving RISs (R-RISs) have been proposed for efficient three-dimensional (3D) localization without intervention from base stations or access points [10].

This paper focuses on RIS-based localization in a tracking scenario, extending previous approaches that mainly considered stationary UEs. The contributions of this work are

- The design of a measurement engine that utilizes a stateof-the-art carrier-aided code phase-based navigation receiver and incorporates a passive correlation-based anglelocked loop (ALL) approach to estimate the TOA and AOA, respectively.
- The deployment of an extended Kalman filter (EKF)-based RIS-aided navigation framework that estimates the 3D position and velocity of a mobile UE using TOA and AOA measurements, with a RIS whose phase profile is optimized to maximize the UEs' SNRs.
- Demonstration of the navigation solution accuracy in Monte-Carlo simulations, where performance in different scenarios involving pedestrians, ground vehicles, and unmanned aerial vehicles (UAVs) is assessed.

II. METHODOLOGY

A. Localization Scenario

We consider a 3-D localization scenario with I single-antenna UEs, U single-antenna BSs, and an $N=N_x\times N_y$

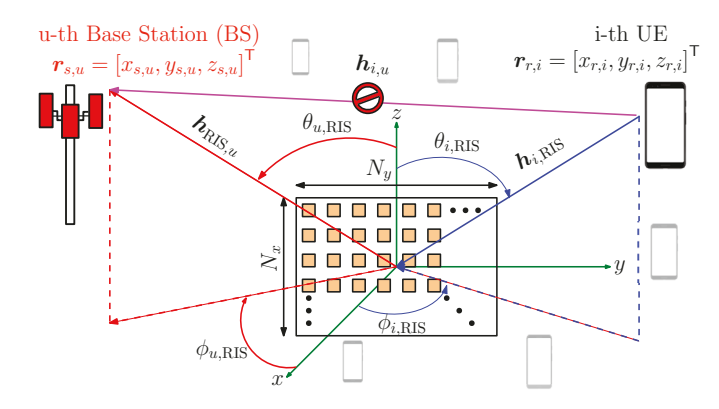


Fig. 1. Localization Scenario

element rectangular RIS. The i-th UE and the u-th BS are located at $\boldsymbol{r}_{r,i} = [x_{r,i},y_{r,i},z_{r,i}]^\mathsf{T}$ and $\boldsymbol{r}_{s,u} = [x_{s,u},y_{s,u},z_{s,u}]^\mathsf{T}$, respectively. The RIS is assumed to lie in the yz-plane with a reference point $\boldsymbol{0}_3$, where the location of the n-th element is denoted by $\boldsymbol{r}_{\mathrm{ris},n} = [0,y_{\mathrm{ris},n},z_{\mathrm{ris},n}]^\mathsf{T}$. The RIS elements are regularly spaced with inter-element spacing $d = \lambda/2$ in both dimensions. Figure 1 depicts the localization scenario.

B. Signal and Channel Model

A mm-wave uplink OFDM transmission is considered in which the LOS signal is blocked and only the RIS reflected signal (also known as the virtual LOS in the literature) is received. The complex baseband signal received by the u-th BS from the i-th UE can be expressed as

$$r_i^u(t) = \sqrt{P}\alpha_i^{(u)} s_i(t - \tau_i^{(u)}) + w(t),$$
 (1)

where P is the transmit power, $s_i(t)$ is the known OFDM signal of the i-th UE, w(t) is zero-mean white Gaussian noise with variance σ_n^2 , $\tau_i^{(u)} = \frac{\|r_{r,i}\|_2 + \|r_{s,u}\|_2}{c}$ is the reflected UE-RIS-BS path delay, and c is the speed of light. The complex channel gain $\alpha_i^{(u)}$ is modeled geometrically in the mm-wave regime [14] as

$$\alpha_{i}^{(u)} = e^{-j2\pi f_{c}\tau_{i}^{(u)}} \frac{\lambda^{2}}{16\pi^{2} \|\boldsymbol{r}_{r,i}\|_{2} \|\boldsymbol{r}_{s,u}\|_{2}} \boldsymbol{h}_{\text{RIS},u}^{\mathsf{T}} \boldsymbol{\Omega} \boldsymbol{h}_{i,\text{RIS}}, \quad (2)$$

where f_c is the carrier frequency, $h_{RIS,u}$ is the $N \times 1$ RIS to u-th BS response vector, $h_{i,RIS}$ is the i-th UE to RIS response vector, and Ω is an $N \times N$ diagonal matrix whose diagonal elements correspond to the electronically controlled RIS element responses that are optimized depending on the current estimates of the UE locations. The response vector $h_{RIS,u}$ is expressed as

$$[\boldsymbol{h}_{\text{RIS},u}]_n = e^{-j\boldsymbol{r}_{\text{ris},n}^{\mathsf{T}}\boldsymbol{k}(\phi_{\text{RIS},u},\theta_{\text{RIS},u})}, \quad n \in \{0, 1, \cdots, N-1\},$$
(3)

where $\phi_{\text{RIS},u}$ and $\theta_{\text{RIS},u}$ are the azimuth and elevation angles corresponding to the angle of departure of the signal from the RIS to the u-th BS, and $k(\phi,\theta)$ is the wavevector given by

$$\mathbf{k}(\phi, \theta) = -\frac{2\pi}{\lambda} \begin{bmatrix} \sin(\theta)\cos(\phi) \\ \sin(\theta)\sin(\phi) \\ \cos(\theta) \end{bmatrix}. \tag{4}$$

The response vector $h_{i,RIS}$ is similarly written as

$$[\boldsymbol{h}_{i,\text{RIS}}]_n = e^{-j\boldsymbol{r}_{\text{ris},n}^{\mathsf{T}}\boldsymbol{k}(\phi_{i,\text{RIS}},\theta_{i,\text{RIS}})}, \quad n \in \{0, 1, \cdots, N-1\}.$$
(5)

The diagonal elements of the RIS phase profile matrix Ω are defined by

$$\boldsymbol{w} = \operatorname{diag}(\boldsymbol{\Omega}) = \left[e^{jw_0}, e^{jw_1}, \cdots, e^{jw_{N-1}} \right]^{\mathsf{T}} . \tag{6}$$

C. Measurement Engine

Here we discuss the measurement engine which comprises two parts: (i) TOA estimation and (ii) AOA estimation. To estimate the TOA from the received OFDM signals, the engine adopts a state-of-the-art carrier-aided code-phase-based cellular navigation receiver [15]. The receiver deploys a phase-locked loop (PLL) to track the carrier phase and a carrier-aided delay-locked loop (DLL) to track the code phase. The proposed system builds on top of this receiver design to passively estimate the AOA using a correlation-based ALL.

1) AOA Estimation: Here we present a novel method for estimating the azimuth and elevation angles between the UE and the RIS using a passive AOA estimator. The proposed approach leverages the correlation properties of the OFDM uplink signals at the BS. It assumes that the BS has prior knowledge of the channel coefficients $h_{RIS,u}^{\mathsf{T}}$ and the RIS phase profile Ω , which is feasible in an uplink scenario where the BS and RIS positions are known. The proposed method aims to estimate the UE's position-dependent parameter, $h_{i,RIS}$ in (2), which is a function of the UE-RIS azimuth and elevation angles $(\phi_{i,RIS}, \theta_{i,RIS})$, as described in (5).

To achieve this, a UE-RIS AOA search is performed during the system initialization, with a predefined resolution. Fig. 2 illustrates a sample output of this search, where the normalized autocorrelation function (ACF) exhibits peaks at the true AOA. The accuracy of the initial AOA estimate depends on the chosen search resolution, which has implications for the computational complexity. The proposed AOA estimator overcomes the aforementioned challenges, and its design is inspired by the design of the DLL, which employs a discriminator with early and late correlation measurements based on delayed and advanced replicas of the prompt code, respectively [16]. The difference between the early and the late correlators produces a so-called S-curve, whose zero crossings are tracked by the DLL to estimate the current error, which is then fed back to the local code generation block to correct the previous estimate of the incoming code delay.

To design the AOA discriminator, we first conduct a Monte Carlo AOA error analysis assuming a single BS, RIS, and UE. The simulation settings can be found in Table I. The AOA errors vs the normalized ACF from over 1000 iterations are shown in Fig. 3. These errors are analyzed to design a normalized early-minus-late (eml) angle discriminator by obtaining the S-curves for both azimuth and elevation for different eml angles denoted by $a_{\rm eml}$. The region of interest for AOA estimation is defined to be $\pm 5^{\circ}$, which represents the change among the AOAs between two consecutive measurements. The linearity of each of the S-curves was assessed

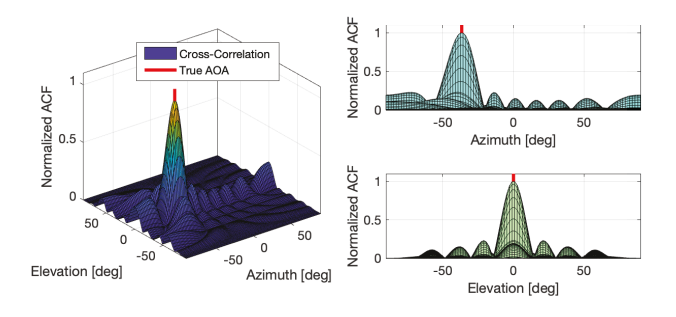


Fig. 2. Sample output of the initial UE-RIS AOA search.

TABLE I
AOA DISCRIMINATOR MONTE-CARLO SETTINGS

Parameter	Value	Description
$x_{\rm range}$	[-2.5, 2.5] km	Geometric range in x direction
$y_{\rm range}$	[-2.5, 2.5] km	Geometric range in y direction
$z_{ m range}$	[-50, 50] m	Geometric range in z direction, relative heights of BS, RIS, UE
f_c	28 GHz	Carrier frequency
B	100 MHz	OFDM Signal Bandwidth
$t_{ m frame}$	10 ms	Typical 4/5G frame duration
sc	15 kHz	OFDM subcarrier spacing
N	64	Number of RIS elements

and a linear RMSE fit was computed. A value of $a_{\rm eml} \triangleq 1^{\circ}$ gave the most accurate open-loop estimates, and the resulting azimuth and elevation eml discriminator performance can be seen in Figures 4 and 5, respectively.

In addition to the angle discriminator, the ALL consists of a loop filter gain K with a noise-equivalent bandwidth $B_{n,\mathrm{ALL}}=\frac{K}{4}\equiv 0.05$ Hz. The block diagram of the overall measurement engine is depicted in Fig. 6.

D. RIS Phase Profile Design

As with any signal-based localization approach, the estimation error is inversely proportional to the received signal-to-noise-ratio (SNR) [16]. The SNR of the i-th UE at the u-th BS antenna is defined as

$$SNR_i^{(u)} \triangleq P \frac{||\alpha_i^{(u)}||^2}{\sigma_r^2}.$$
 (7)

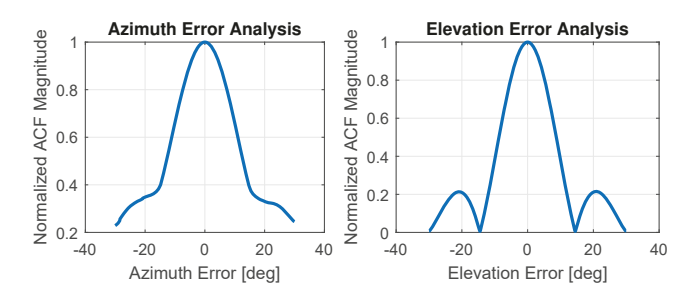


Fig. 3. AOA errors vs ACF.

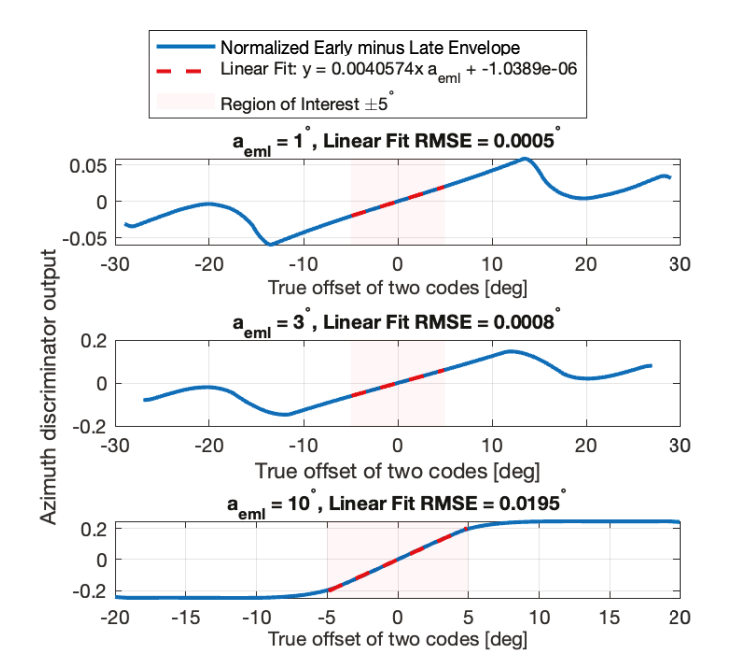


Fig. 4. Azimuth early-late discriminator.

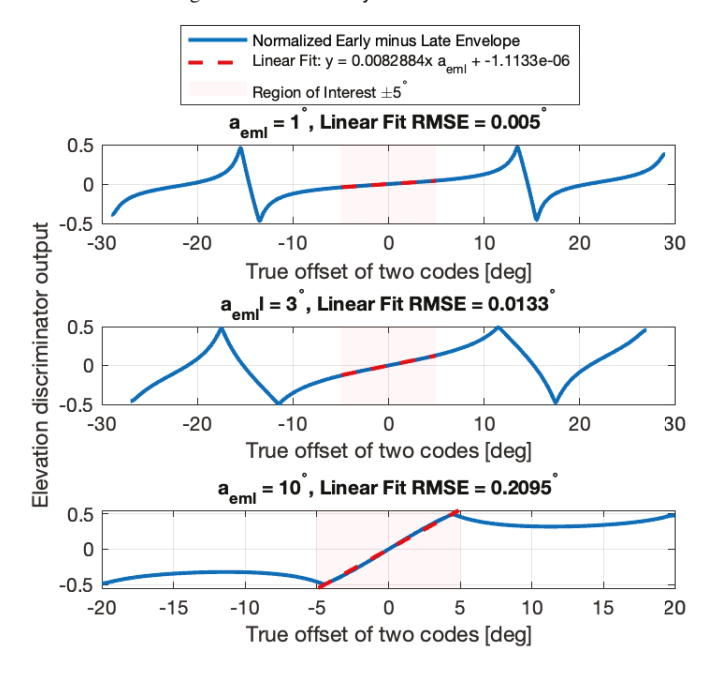


Fig. 5. Elevation early-late discriminator.

Assuming a single BS that is controlling the RIS phase profile, and in the presence of multiple UEs, the optimization of the RIS phase profile, Ω , is formulated to maximize the minimum SNR among all UEs, which can be formulated as

$$\underset{\Omega}{\text{maximize}} \quad \min \{ SNR_i^{(u)} \}_{i=1}^{i=I}$$
 (8)

subject to
$$|w_j| = 1$$
, for $j = 1, \dots, N$. (9)

E. EKF

Separate EKFs are deployed to estimate the UEs' 3D positions and velocities using the TOA and AOA measurements.

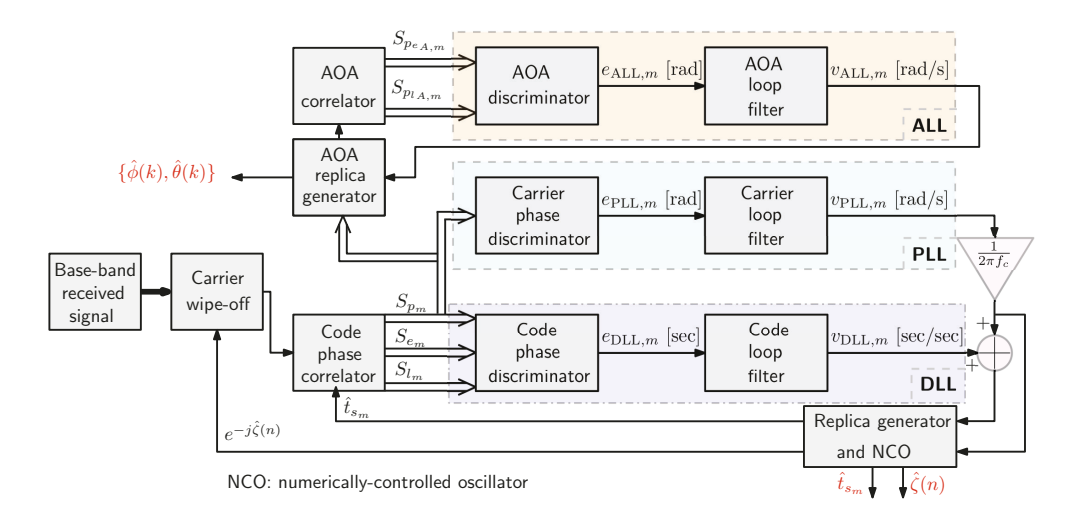


Fig. 6. Overall localization approach.

The EKF state vector for the i-th UE is expressed as

$$\boldsymbol{x}_i \triangleq \begin{bmatrix} \boldsymbol{r}_{r,i}^\mathsf{T}, \dot{\boldsymbol{r}}_{r,i}^\mathsf{T} \end{bmatrix}^\mathsf{T}. \tag{10}$$

The UE's motion is assumed to evolve according to a nearly constant velocity dynamic with process noise vector $\tilde{\boldsymbol{w}}_r = \left[\tilde{w}_x, \tilde{w}_y, \tilde{w}_z\right]^\mathsf{T}$, whose elements are modeled as zero-mean and mutually independent white noise processes with power spectral densities \tilde{q}_x , \tilde{q}_y , and \tilde{q}_z , respectively [15].

III. RESULTS

In this section, a Monte Carlo simulation is performed to study the navigation performance of the proposed system for three scenarios involving pedestrians, ground vehicles, and UAVs. The simulation settings are the same as in Table I except for different initial velocity ranges $v_{\rm init}$, and UE dynamics parameters $[q_x, q_y, q_z]$, according to the scenario of interest. Table II summarizes the parameter ranges for the different cases. The number of users is chosen to be 10; the initial covariance matrix was set to $\mathbf{P}(0|0) \triangleq \mathrm{diag}([\mathbf{10}_{1\times 3}^\mathsf{T}, \mathbf{5}_{1\times 3}^\mathsf{T}]^\mathsf{T})$, and the measurement noise covariance matrix was chosen to be $\mathbf{R} \triangleq \mathrm{diag}([1,5,5]^\mathsf{T})$.

The Monte Carlo analysis was run for 500 trials each with a random set of parameters selected according to the ranges provided in Table II. The average empirical cumulative distribution functions (CDFs) of the positioning errors for the different scenarios over all iterations and users are depicted in Figure 7. It can be seen that the best accuracy was achieved for pedestrian dynamics, while the ground vehicle had comparable but overall less accuracy. This is expected due to the higher dynamic stress introduced by the ground vehicle's dynamics resulting in increased process and measurement noise.

IV. CONCLUSION

This paper introduced a novel approach to localization in a millimeter-wave uplink cellular environment using a RIS, specifically targeting mobile UEs. The proposed approach develops a measurement engine utilizing a state-of-the-art carrier-aided code phase-based 5G navigation receiver and incorporates a passive correlation-based ALL for TOA and

TABLE II
DYNAMICS PARAMETERS FOR DIFFERENT PLATFORMS

Platform	Parameter	Value
	$v_{ m init}$	[0, 2.5] m/s
Pedestrian	$q_x \& q_y$	$[0, 1.44] \text{ m/s}^2$
	q_z	$[0, 1] \text{ m/s}^2$
	$v_{ m init}$	[0, 50] m/s
Ground Vehicle	$q_x \& q_y$	$[0, 5] \text{ m/s}^2$
	q_z	$[0, 2] \text{ m/s}^2$
	$v_{ m init}$	[0, 25] m/s
UAV	$q_x \& q_y$	$[0, 3] \text{ m/s}^2$
	q_z	$[0, 4] \text{ m/s}^2$

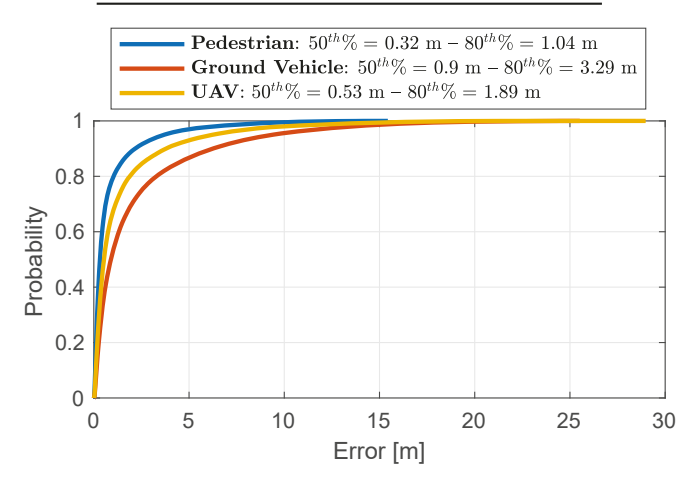


Fig. 7. Empirical CDF of positioning errors for different platforms.

AOA estimation, respectively. Additionally, we deployed an EKF-based RIS-aided navigation framework to estimate the 3D position and velocity of the mobile UEs. The navigation accuracy of the proposed system was assessed via Monte Carlo simulations across varied scenarios, including pedestrians, ground vehicles, and UAVs. The simulations underscored the potential and efficacy of the proposed navigation system, showcasing its ability to yield sub-meter-level to meter-level positioning accuracies for different scenarios.

REFERENCES

- A. Abdallah, K. Shamaei, and Z. Kassas, "Assessing real 5G signals for opportunistic navigation," in *Proceedings of ION GNSS Conference*, 2020, pp. 2548–2559.
- [2] Z. Kassas, J. Morton, F. V. Diggelen, J. Spilker, B. Parkinson, S. Lo, and G. Gao, Position, navigation, and timing technologies in the 21st century: Integrated satellite navigation, sensor systems, and civil applications, Volume 1. Wiley-IEEE, 2021, vol. 2, pp. 1381–1412.
- [3] J. Khalife and Z. Kassas, "On the achievability of submeter-accurate UAV navigation with cellular signals exploiting loose network synchronization," *IEEE Transactions on Aerospace and Electronic Systems*, vol. 58, no. 5, pp. 4261–4278, 2022.
- [4] A. Abdallah, J. Khalife, and Z. Kassas, "Exploiting on-demand 5G downlink signals for opportunistic navigation," *IEEE Signal Processing Letters*, 2023.
- [5] 3GPP, "NG radio access network (NG-RAN): Stage 2 functional specification of user equipment (UE) positioning in NG-RAN," 3rd Generation Partnership Project (3GPP), TR 38.305 V16.1.0, July 2020.
- [6] E. Basar, M. D. Renzo, J. D. Rosny, M. Debbah, M. Alouini, and R. Zhang, "Wireless communications through reconfigurable intelligent surfaces," *IEEE Access*, vol. 7, pp. 116753–116773, 2019.
- [7] M. D. Renzo, A. Zappone, M. Debbah, M. Alouini, C. Yuen, J. D. Rosny, and S. Tretyakov, "Smart radio environments empowered by reconfigurable intelligent surfaces: How it works, state of research, and the road ahead," *IEEE Journal on Selected Areas in Communications*, vol. 38, no. 11, pp. 2450–2525, 2020.
- [8] Y. Liu, X. Liu, X. Mu, T. Hou, J. Xu, M. D. Renzo, and N. Al-Dhahir, "Reconfigurable intelligent surfaces: Principles and opportunities," *IEEE Communications Surveys & Tutorials*, vol. 23, no. 3, pp. 1546–1577, 2021
- [9] K. Keykhosravi, M. Keskin, S. Dwivedi, G. Seco-Granados, and H. Wymeersch, "Semi-passive 3D positioning of multiple RIS-enabled users," *IEEE Transactions on Vehicular Technology*, vol. 70, no. 10, pp. 11073–11077, 2021.
- [10] J. He, A. Fakhreddine, C. Vanwynsberghe, H. Wymeersch, and G. Alexandropoulos, "3D localization with a single partially-connected receiving RIS: Positioning error analysis and algorithmic design," arXiv preprint arXiv:2212.02088, 2022.
- [11] A. Albanese, P. Mursia, V. Sciancalepore, and X. Costa-Pérez, "PAPIR: Practical RIS-aided localization via statistical user information," in International Workshop on Signal Processing Advances in Wireless Communications (SPAWC), 2021, pp. 531–535.
- [12] T. Ma, Y. Xiao, X. Lei, W. Xiong, and Y. Ding, "Indoor localization with reconfigurable intelligent surface," *IEEE Communications Letters*, vol. 25, no. 1, pp. 161–165, 2020.
- [13] M. Rahal, B. Denis, K. Keykhosravi, B. Uguen, and H. Wymeersch, "RIS-enabled localization continuity under near-field conditions," in IEEE International Workshop on Signal Processing Advances in Wireless Communications (SPAWC), 2021, pp. 436–440.
- [14] A. Shahmansoori, G. Seco-Granados, and H. Wymeersch, "Power allocation for OFDM wireless network localization under expectation and robustness constraints," *IEEE Transactions on Wireless Communi*cations, vol. 16, no. 3, pp. 2027–2038, 2017.
- [15] A. Abdallah and Z. Kassas, "UAV navigation with 5G carrier phase measurements," in *Proceedings of ION GNSS Conference*, 2021, pp. 3294–3306.
- [16] P. Misra and P. Enge, Global Positioning System: Signals, Measurements, and Performance, 2nd ed. Ganga-Jamuna Press, 2010.